Proceedings of the 11th Brazilian Congress of Thermal Sciences and Engineering – ENCIT 2006
Braz. Soc. of Mechanical Sciences and Engineering – ABCM, Curitiba, Brazil, Dec. 5-8, 2006

Paper CIT06-0298

HIGH-ORDER NON-UNIFORM GRID SCHEMES FOR NUMERICAL INVESTIGATION OF COMPRESSIBLE SHEAR LAYERS

Ricardo A. C. Germanos
USP - Universidade de São Paulo
Escola de Engenharia de São Carlos - Departamento de Engenharia Aeronáutica
Av. Trabalhador São Carlense, 400 - SP - 13566-590, Brazil
gercop@sc.usp.br

Stefan Wernz
The University of Arizona
Department of Aerospace and Mechanical Engineering
1130 North Mountain Ave., Tucson, Arizona, USA
wernzs@email.arizona.edu

Hermann F. Fasel
The University of Arizona
Department of Aerospace and Mechanical Engineering
1130 North Mountain Ave., Tucson, Arizona, USA
faselh@email.arizona.edu

Marcello A. Faraco de Medeiros
USP - Universidade de São Paulo
Escola de Engenharia de São Carlos - Departamento de Engenharia Aeronáutica
Av. Trabalhador São Carlense, 400 - SP - 13566-590, Brazil
marcello@sc.usp.br

Abstract. *The engineering research and design requirements of today pose great challenges in computer simulation to engineers and scientists who are called on to analyze phenomena in continuum mechanics. The study of hydrodynamic instability is a subject well researched, and comes in numerous practical situations such as aerodynamics, combustions and environmental engineering. In the current work, the instability of a compressible free shear layer at relatively low Reynolds numbers was investigated. In the aerospace context, important applications involve compressible flows at relatively low Reynolds numbers. Among them, the flow on gas turbine blades and the flow on high lift devices such as slats and flaps at high angle of attack are particularly important. In aerodynamic applications at low Reynolds numbers, often a substantial portion of the flow is in the transition regime, or in the initial turbulent stages. Despite the extensive research carried out in the field, there are various aspects of the transition process that require further studies. The transition in compressible flows is an example. Here, simulations of compressible Navier-Stokes equations have been performed. Spatial derivatives in these equations were discretized using of a sixth-order finite-difference method. In order to solve the time derivatives a fourth-order Runge-Kutta method was adopted. As the last step of the integration scheme, a compact filter was applied to remove short length scales in the streamwise and normal directions. Moreover, the compact schemes were modified to work with non-uniform grids. In this case, a stretching in y-direction was implemented with the objective to reduce the sound waves generated by shear region and to improve the resolution in the interior of the domain. The numerical investigation starts with an analysis of the amplification rate in linear regime. Tests were also performed in the non-linear regime and it was possible to reproduce the vortex roll-up and pairing. Through these results, the effect of the Mach number on the evolution of shear instabilities was analyzed.*

keywords: *hydrodynamic instability, transition, compressible shear layer, compact schemes, grid stretching*

1. Introduction

The study of transition in mixing layers has constituted one of the main research themes in turbulence over the last thirty years. This flow types is found in many situations in nature like in atmospheric flows, volcanic eruptions, stellar jets and in industrial applications such as gas turbine combustors, airfoil wakes and rocket

exhausts. A detailed understanding of the physics of free shear layers is essential for the development of new turbulence and mixing models. Improved models of mixing in free shear layers will lead to a better capability of predicting chemical reactions and controlling pollutant emissions, for example from oil and gas burners in power generation plants. Also progress in space research is dependent on developing more efficient propulsion systems, and vehicles capable of carrying a higher payload into orbit.

A mixing layer develops at the interface of two-stream of different speeds. The velocity profile formed possesses an inflection point that is unstable to infinitesimal disturbances. This phenomenon called Kelvin-Helmholtz instability is inviscid and is responsible for the formation of vorticity structures aligned in the lateral direction. This behavior was observed laboratory experiments carried out by Birch and Eggers, 1973 and Brown and Roshko, 1974. According to Lesieur, 1997 due to the vorticity concentration, the recognizable form, and the unpredictability in relation to the location in the time and space, these vortical structures exhibit all the characteristics of coherent structures.

In addition to Kelvin-Helmholtz instability vortex, experimental works presented by Bernal and Roshko, 1986 and numerical works published by Metcalfe *et al.*, 1987 put in evidence the existence of one secondary instability that causes, in the stagnation area between the Kelvin-Helmholtz vortices, intense longitudinal counter-rotative vortices. These longitudinal vortices, denominated hairpins are easily identifiable in a transverse cut in the form of a mushroom and responsible for the largest portion of the transfer of mass, momentum and energy conservation in transitional and turbulent flows.

Studies of the linear stability of compressible mixing layers presented by Lessen *et al.*, 1966, Blumen *et al.*, 1975 show a strong reduction in the amplification rate of two-dimensional disturbances in the flow as Mach number is increased. In compressible mixing layers there are two flows with different speeds, and consequently, with different characteristic Mach numbers. Therefore the representative parameter is the convective Mach number (Papamoschou and Roshko, 1988). Experiments show that this parameter characterizes the flow correctly for Mach number below 0.6. Simulations carried out by Sandham and Reynolds, 1989 show that for convective Mach number lower than 0.6 the two-dimensional disturbances is the most strongly amplified whilst for convective Mach number above to 0.6, the oblique waves are dominant in the flow and the mixing layer will have a highly three-dimensional structure.

These kinds of flows possess wide range of space and time scales and therefore require high accuracy in the numerical solution. This accuracy requirement can be achieve by the use of spectral methods (Canuto *et al.*, 1987). These methods can be used to assure that all relevant scales are captured, but high-order finite-difference are also able to represent short length scales with good accuracy. Lele, 1992, emphasizes the importance of using high-order schemes for first and second derivatives. Mahesh, 1998, presents high-order finite-difference schemes, introducing a method that, using the same stencil is more accurate than the standard Padé schemes. A disadvantage of his method is that it requires the solution of first and second derivatives simultaneously. Souza *et al.*, 2002a; Souza *et al.*, 2002b, used high-order compact methods for transition phenomenon problems. In these studies it was investigated the propagation of the Tollmien-Schlichting waves in incompressible flows.

In the present work, a high-order compact scheme was adopted to solve the spatial derivatives (Lele, 1992). The computational domain is periodic in x-direction. In the y-direction, the free-slip condition was adopted according to Medeiros *et al.*, 2000 and Souza, 2003. Emphasizing that this boundary condition produces accurate results for a sufficiently large distance from the mixing layer. Another possibility would be to use an exponential decay condition, except that this method is only rigorously correct in the linear regime. Thompson, 1987 presents non-reflecting boundary conditions whereas the idea of these boundary conditions is to consider the characteristic form of the Euler equation at the boundary. Finally, to solve the temporal derivatives, the time-advancement is obtained by using a high-order Runge-Kutta scheme in agreement with Williamson, 1980. This scheme is conditionally stable and therefore small time increments are required to assure that the stability criterion is satisfied. A similar scheme was used by Kloker *et al.*, 1993.

The linear and non-linear temporal evolution of two-dimensional instability waves in the unconfined mixing layer was simulated. Tests based on the linear stability theory were used to validate the code. In these tests, the growth rates obtained in the present simulations was compared with results from other numerical works. Simulations in the non-linear regime were also performed. The long term objective of this work is the simulation of compressible boundary layer phenomena, such as the present studied, the authors of this work consider essential to verify the code first with as the case of mixing layer and acoustic wave problems. Previous works present other verification tests with the simulation of the linear acoustic wave problem (Germanos *et al.*, 2004).

The organization of the paper is as follows. Section 2 presents the formulation of the governing equations adopted in the current work. Details of the numerical method are described in the section 3. Section 4 shows a numerical simulation of the mixing layer instability. The last section presents the conclusion of this work.

2. Formulation

In this study, the governing equations are the compressible, Navier-Stokes equations according to Sandham and Reynolds, 1991 and Eibler and Bestek, 1996. They consist of the momentum equations for the velocity components (u,v) in the streamwise direction (x) and normal direction (y)

$$\frac{\partial \rho u_i}{\partial t} + \frac{\partial \rho u_i u_j}{\partial x_j} = -\frac{\partial p}{\partial x_i} + \frac{\partial \tau_{ij}}{\partial x_j}, \tag{1}$$

and the continuity and energy equation

$$\frac{\partial \rho}{\partial t} + \frac{\partial \rho u_j}{\partial x_j} = 0, \tag{2}$$

$$\frac{\partial E}{\partial t} + \frac{\partial u_j (E+p)}{\partial x_j} = -\frac{\partial q_j}{\partial x_j} + \frac{\partial u_j \tau_{ij}}{\partial x_j}, \tag{3}$$

where x_i are the Cartesian coordinates (x,y), t is the time, u_i are the velocity components (u,v), ρ is the density and p is the pressure. The non-dimensional constitutive relations for a Newtonian fluid with Fourier heat conduction are

$$\tau_{ij} = \frac{1}{Re}\left(\frac{\partial u_i}{\partial x_j} + \frac{\partial u_j}{\partial x_i} - \frac{2}{3}\frac{\partial u_k}{\partial x_k}\delta_{ij}\right), \tag{4}$$

$$q_i = -\frac{1}{(\gamma-1)M^2 PrRe}\frac{\partial T}{\partial x_j}. \tag{5}$$

The total energy E_t is given by $E_t = \rho\left(e + \frac{u^2+v^2}{2}\right)$, where e is the internal energy. The Reynolds number of the flow is defined as

$$Re = \frac{\rho_1 \, U_1 \, \delta^*_{\omega_0}}{\mu}, \tag{6}$$

where U is the velocity, ρ is the density and μ is the dynamic viscosity of the flow. The variable $\delta^*_{\omega_0}$ is the vorticity thickness of the initial velocity given by

$$\delta^*_{\omega_0} = \frac{U_1^* - U_2^*}{|d\bar{u_0}^*/dy^*|_{max}}, \tag{7}$$

where the subscript 1 and 2 refers to the upper ($y > 0$) and lower ($y < 0$) free stream, respectively. The perfect-gas law for pressure and temperature in this non-dimensional scheme is

$$p = (\gamma - 1)\rho e, \tag{8}$$

$$T = \frac{\gamma M^2 p}{\rho}, \tag{9}$$

where γ is the relation of the specific heat. The Prandtl number $Pr = \frac{c_p \, \mu}{k}$ was assumed constant $Pr = 1$, where k is the thermal conductivity.

These equations were defined with the following non-dimensionalization scheme

$$u_i = \frac{u_i^*}{U_1}, \quad \rho = \frac{\rho^*}{\rho_1}, \quad p = \frac{p^*}{\rho_1 \, U_1^2}, \quad t = \frac{t^* U_1}{\delta^*_{\omega_0}}, \quad x_i = \frac{x_i^*}{\delta^*_{\omega_0}}, \quad \alpha = \alpha^* \delta^*_{\omega_0}, \quad \omega = \frac{\omega^* \delta^*_{\omega_0}}{U_1}, \tag{10}$$

where α^* is the dimensional wavenumber of the disturbed flow, ω^* is the dimensional frequency of the flow.

3. Methodology

3.1. Initial Condition

The first step for simulating instabilities in a shear layer is to implement a initial velocity profile. In the velocity profile adopted in this work, the upper part of the stream travels faster than the lower part. The choice of transition between these two different speeds is crucial in order not to generate waves in the first time steps, which could then be reflected on edges. In this work, the two-dimensional problem was considered because it has been shown that for low Mach numbers (typically under 0.4), the dominant instability mode for the shear layer is two-dimensional and that three-dimensional instabilities only become important for high Mach numbers.

Many different velocity profiles have been proposed in the literature for modelizing a shear layer. Rayleigh, 1880 has demonstrated that the profile has to have an inflexion point to be unstable. This means that disturbances will be amplified and lead to the formation of vortice structures, which will also be in an unstable equilibrium and therefore will create some pairing until the energy has dispersed through viscous dissipation. The profile used in this numerical work corresponds in an hyperbolic tangent function that uses a velocity means at upper and lower of the free stream flow to calculate the velocity in coordinate y.

Along with the velocity profile the disturbance flow has to be defined. Numerical errors engender perturbations, which are sufficient to suscitate such instabilities in the shear layer flow but only after a very long time. The formation of vortice structures can be largely accelerated by using some disturbance functions, which correspond to the eigenfunctions of stream. This idea of exciting a stream adding to the mean flow a little disturbance to accelerated the process is widely spread in the scientific community. This technique was often used by Colonius *et al.*, 1997 for spatial development, Michalke, 1964 for temporal development in incompressible flows and Sandham and Reynolds, 1991 for compressible case.

Thus the variables were decomposed into two parts: the temporary mean and a small disturbance. This way the primitive variables can be rewritten in the following way

$$\begin{aligned} u(x,y,z,t) &= u_0(y) + u', \\ v(x,y,z,t) &= v', \\ \rho(x,y,z,t) &= 1 \\ T(x,y,z,t) &= T_0(y) \\ p(x,y,z,t) &= \tfrac{1}{\gamma M^2}. \end{aligned} \tag{11}$$

where the subscript $(_0)$ refers to a temporary mean flow and $(')$ refers to a small disturbance. The mean flow is invariant in the streamwise direction and the component (v) of the mean velocity is null. In other words, the mean flow is locally parallel.

In this work the velocity profile is defined as

$$\bar{u}_0(y) = \frac{U_1 + U_2}{2} + \frac{U_1 - U_2}{2} \tanh(\frac{2y}{\delta_{\omega_0}}). \tag{12}$$

The vorticity thickness is given by equation 7. This profile has often been used because it has the great advantages of being analytical. Consequently, speed can be calculated exactly for each value of y. The derivatives of this function are known as well. The tangent profile was used by Michalke, 1964 and by Fortuné, 2000 in their papers about shear layer developing in time and by Colonius *et al.*, 1997 for shear layers developing in space. A disadvantage of using the tangent profile is that it neither satisfies the momentum equation nor the energy equation and, therefore, it can cause an impact in first time steps in the numerical integration of the temporal primitives variables of Navier-Stokes equation.

The initial mean temperature profile can be specified as a solution to the compressible boundary layer energy equation (White, 1974), assuming unity Prandtl number. For the antisymmetric mean velocity profile considered here, and with equal free stream temperatures the general relation of Crocco-Busemann is given by

$$\bar{T}_0(y) = 1 + M_c^2 \frac{\gamma - 1}{2}(1 - \bar{u}_0^2(y)), \tag{13}$$

This relation assumes parallel flow. It is noted that for all simulations here the convective Mach number M_c is equal to the free stream Mach number M. Uniform pressure is assumed for the initial mean flow ($p_0 = \frac{1}{\gamma M^2}$), so the mean density profile is calculated with equation 8.

The disturbances can be generalized by

$$u'(x,y,t) = \phi_1(y) e^{i(\alpha x - \omega t)} + \phi_2(y) e^{i\frac{1}{2}(\alpha x - \omega t)} \tag{14}$$

where α refers to the spatial wavenumber and ω to the frequency of the disturbance flow. The variable ϕ_1 correspond to an eigenfunction of the stream and ϕ_2 refers to the first subharmonic mode. The eigenfunction u' is a function of the y-coordinate only. For the time-developing shear layer problem, disturbances grow in time. Thus, the wavenumber α is real. The streamwise wavelength of a disturbance is given by $L_x = 2\pi/\alpha$, the phase speed by $c_r = \omega_r/\alpha$ and the amplification rate by ω_i.

In this work the eigenfunctions were approximated by exponential functions (Michalke, 1964). Exponential functions are convenient because they decrease really quick and respect the boundary conditions $u'(^-_+\infty) = 0$. Furthermore, those functions can easily be analytically differentiated. For find the disturbance flow some assumptions were made. First the flow is considered inviscid because mechanism of instability is inviscid and the only effect of viscosity is to damp the growing disturbances. Second the flow is considered incompressible, which is only true for very small Mach numbers. Based on these hypotheses the disturbance flow can be defined as

$$u' = \frac{2\sigma y}{(\alpha_1\alpha_2)}\left[A_1\sin(\alpha_1 x)\alpha_2 + A_2\sin(\alpha_2 x)\alpha_1\right]\exp(-\sigma y^2), \tag{15}$$

$$v' = \left[A_1\sin(\alpha_1 x) + A_2\sin(\alpha_2 x)\right]\exp(-\sigma y^2), \tag{16}$$

where A is the amplitude, α is the wavenumber and σ is the spread of the disturbance in the y-direction. The subscript 1 refers to the dominant mode fundamental and subscript 2 refers to the subharmonic mode.

3.2. Boundary Conditions

In these simulations we are considering the problem of an unbounded compressible mixing layer. The infinite extent could be obtained by using a mapping function, but this would lead to poor resolution of the flow far away from the mixing layer. In particular, sound waves would propagate into regions of the computational domain where these waves would be poorly resolved, and might be reflected back and contaminate the main flow. Thus, we require boundary conditions which simulate an infinite domain, even though the computational domain is finite. In order to reproduce this mechanism, the appropriate specification of boundary conditions represents an important task for the development of computational simulations. At the free stream boundary the flow was assumed to be irrotational. This assumption is usually satisfied to machine precision in numerical calculations. Thus, the normal component of velocity in the free stream is set to zero. This condition satisfies the impermeability conditions. For other primitive variables the first derivatives are set to zero to satisfies the condition of free-slip. These schemes can be seen below

$$\begin{aligned} v &= 0, \\ \tfrac{\partial}{\partial y}(u, w, \rho, p) &= 0. \end{aligned} \tag{17}$$

Ideally, one would like enforcing a vanishing perturbation velocity at a very large distance from the shear layer, but these requires a very large computational domain. For a sufficient large distance form shear layer, this boundary condition should produce accurate results.

Another assumption used in this work is to considered a boundary condition of Roubin that specified the disturbance velocity for normal component as

$$\frac{\partial v}{\partial y} = -\alpha v \tag{18}$$

This condition imposes exponential decay of disturbances at the free-stream. In the case of shear layer, this exponential decay follows from linear stability theory. For sufficiently large distance from the shear zone the solution is quite insensitive to the value of α.

Finally, in x-direction a periodic boundary conditions was used as proceed below.

$$\begin{aligned} f(0) &= f(L), \\ \frac{\partial^\eta f(0)}{\partial x_i^\eta} &= \frac{\partial^\eta f(L)}{\partial x_i^\eta}. \end{aligned} \tag{19}$$

This method was verified through linear acoustic waves problems. Details about these tests can be found in the technical report by Germanos and Medeiros, 2004.

3.3. Numerical Methods

This section presents the numerical method adopted for a time-developing free shear layer problem. These types of flows possess wide range of space and time scales and therefore require high accuracy at the numerical

solution. This requirement of accuracy can be achieve by the use of spectral methods (Canuto *et al.*, 1987). The use of this scheme is restricted to flows in simple domains and with simple boundary conditions. In order to overcome these difficulties an alternative numerical representations can be used as the finite-differences schemes and the finite volume schemes. The advantage of finite volume schemes has advantages in working with complex domains and also with complex boundary conditions. On the other hand the finite-differences schemes is justified by the possibility of the use of more general boundary conditions, although the schemes with high-order of accuracy is also restricted to the problem with simple domains. The advantage of these schemes in relation to finite volume schemes is that high-order approximations can be obtained. These schemes can be classified as explicit or implicit. Although the cost of inverting a banded matrix to obtain the nodal derivatives, the implicit schemes are significantly more accurate for the small scales than explicit schemes with the same stencil width (Collatz, 1966 and Kopal, 1961). Since tridiagonal matrices can be inverted quite efficiently (Strang, 1988), the implicit schemes are extremely attractive when explicit time advancement schemes are used. The most popular of the implicit schemes also called compact schemes is the symmetric sixth order version. These schemes is non-dissipative due to the symmetry.

Here the finite-difference approximation to the derivative of the function is expressed as a linear combination of the given function values on a set of nodes. First a uniformly spaced mesh was considered where the nodes are indexed by i. The independent variable at the nodes is $x_i = ih$ for $0 \leq i \leq N$. In these schemes the value of f'_i possess a dependence with all the nodal values. In general implicit or compact schemes are significantly more accurate for short length scales than explicit schemes (Collatz, 1966 and Kopal, 1961). This increase of accuracy can be reached with the inversion of a tridiagonal matrix to obtain the derivative values. Strang, 1988 presents quite efficient methods to solve linear system like this. Lele, 1992 emphasizes the importance of using methods of high-order and proposes schemes with 6^{th} order approximation in the interior of the mesh whereas at the boundaries and near the boundaries the 3^{rd} and 4^{th} order approximation was used, respectively.

Below, the discretization used in the streamwise and the normal direction are present. The letters i, j represent the grid position in the x and y directions, which varies from 0 to M, N respectively. In the x-direction, the 6^{th} order implicit (compact) derivatives for $0 < i < M$ as follows

$$\begin{bmatrix} 3 & 1 & & & & & 1 \\ 1 & 3 & 1 & & & & \\ & \ddots & \ddots & \ddots & & & \\ & & 1 & 3 & 1 & & \\ & & & \ddots & \ddots & \ddots & \\ & & & & 1 & 3 & 1 \\ 1 & & & & & 1 & 3 \end{bmatrix} \begin{bmatrix} f'_0 \\ f'_1 \\ \vdots \\ f'_i \\ \vdots \\ f'_{M-1} \\ f'_M \end{bmatrix} = \begin{bmatrix} \frac{1}{12dx}(f_{M-1} + 28f_M - 28f_1 - f_2) \\ \frac{1}{12dx}(f_M + 28f_0 - 28f_2 - f_3) \\ \vdots \\ \frac{1}{12dx}(f_{i+2} + 28f_{i+1} - 28f_{i-1} - f_{i-2}) \\ \vdots \\ \frac{1}{12dx}(f_{M-3} + 28f_{M-2} - 28f_M - f_0) \\ \frac{1}{12dx}(f_{M-2} + 28f_{M-1} - 28f_0 - f_1) \end{bmatrix}, \tag{20}$$

The viscous terms in the governing equations require evaluation of successive derivatives, for instance $\frac{\partial}{\partial y}(\frac{\partial u}{\partial y})$. When a spectral method is used there is no loss of accuracy if these derivatives are computed by two applications of a first derivatives. However, with finite-difference methods we find that two applications of a first derivative gives a significantly worse representation of the high wavenumbers than a single second derivative computation. This is because the modified wavenumber (Lele, 1992) goes to zero for the first derivative at high wavenumbers. The solution for this problem is to expand all terms in the y direction and calculate the primitives variables in the non-conservative formulation. Therefore the schemes of second derivatives adopted in this work are

$$\begin{bmatrix} 2 & 11 & & & & & 2 \\ 2 & 11 & 2 & & & & \\ & \ddots & \ddots & \ddots & & & \\ & & 2 & 11 & 2 & & \\ & & & \ddots & \ddots & \ddots & \\ & & & & 2 & 11 & 2 \\ 2 & & & & & 2 & 11 \end{bmatrix} \begin{bmatrix} f''_0 \\ f''_1 \\ \vdots \\ f''_i \\ \vdots \\ f''_{N-1} \\ f''_N \end{bmatrix} = \begin{bmatrix} \frac{1}{4h^2}(3f_{N-1} + 48f_N - 102f_0 + 48f_1 + 3f_2) \\ \frac{1}{4h^2}(3f_N + 48f_0 - 102f_1 + 48f_2 + 3f_3) \\ \vdots \\ \frac{1}{4h^2}(3f_{i-2} + 48f_{i-1} - 102f_i + 48f_{i+1} + 3f_{i+2}) \\ \vdots \\ \frac{1}{12h}(3f_{N-3} + 48f_{N-2} - 102f_{N-1} + 48f_N + 3f_0) \\ \frac{1}{12h}(3f_{N-2} + 48f_{N-1} - 102f_N + 48f_0 + 3f_1) \end{bmatrix}. \tag{21}$$

In the normal direction, a non-periodic scheme was studied. This scheme was used by Souza *et al.*, 2002c. At the boundaries a 5^{th} order asymmetric approximation was proposed, whilst for points near the boundaries the 6^{th} order asymmetric approximation was used. For the interior points, the 6^{th} order symmetric approximation was adopted whereas this scheme satisfies free-slip conditions. In this work an alternative scheme was used. This alternative scheme consist in using a 2^{nd} order approximation at the boundaries and for the points near the boundaries. Tests were performed with both schemes and the results confirm that the numerical scheme is more

stable over time. Details about these tests can be found in the technical report by Germanos and Medeiros, 2006. Emphasizes that these schemes will be used only at the free-stream for a sufficiently distance from the shear zone. This compact scheme for first and second derivatives can be seen below

$$\begin{bmatrix} 1 & & & & & & \\ & 1 & & & & & \\ & \ddots & \ddots & \ddots & & & \\ & & 1 & 3 & 1 & & \\ & & & \ddots & \ddots & \ddots & \\ & & & & & 1 & \\ & & & & & & 1 \end{bmatrix} \begin{bmatrix} f'_0 \\ f'_1 \\ \vdots \\ f'_j \\ \vdots \\ f'_{N-1} \\ f'_N \end{bmatrix} = \begin{bmatrix} \frac{1}{2dy}(-3f_0 + 4f_1 - f_2) \\ \frac{1}{2dy}(-f_0 + f_2) \\ \vdots \\ \frac{1}{12dy}(f_{j+2} + 28f_{j+1} - 28f_{j-1} - f_{j-2}) \\ \vdots \\ \frac{1}{2dy}(-f_{N-2} + f_N) \\ \frac{1}{2dy}(f_{N-2} - 4f_{N-1} + 3f_N) \end{bmatrix}, \quad (22)$$

$$\begin{bmatrix} 1 & & & & & & \\ & 1 & & & & & \\ & \ddots & \ddots & \ddots & & & \\ & & 2 & 11 & 2 & & \\ & & & \ddots & \ddots & \ddots & \\ & & & & & 1 & \\ & & & & & & 1 \end{bmatrix} \begin{bmatrix} f''_0 \\ f''_1 \\ \vdots \\ f''_i \\ \vdots \\ f''_{N-1} \\ f''_N \end{bmatrix} = \begin{bmatrix} \frac{1}{h^2}(f_0 - 2f_1 + f_2) \\ \frac{1}{h^2}(f_0 - 2f_1 + f_2) \\ \vdots \\ \frac{1}{4h^2}(3f_{i-2} + 48f_{i-1} - 102f_i + 48f_{i+1} + 3f_{i+2}) \\ \vdots \\ \frac{1}{h^2}(f_{N-2} - 2f_{N-1} + f_N) \\ \frac{1}{h^2}(f_{N-2} - 2f_{N-1} + f_N) \end{bmatrix}. \quad (23)$$

The schemes above were modified to work with free-slip condition as proceeds below

$$\begin{bmatrix} 1 & & & & & & \\ & 1 & & & & & \\ & \ddots & \ddots & \ddots & & & \\ & & 1 & 3 & 1 & & \\ & & & \ddots & \ddots & \ddots & \\ & & & & & 1 & \\ & & & & & & 1 \end{bmatrix} \begin{bmatrix} f'_0 \\ f'_1 \\ \vdots \\ f'_j \\ \vdots \\ f'_{N-1} \\ f'_N \end{bmatrix} = \begin{bmatrix} 0.0 \\ \frac{1}{2dy}(-f_0 + f_2) \\ \vdots \\ \frac{1}{12dy}(f_{j+2} + 28f_{j+1} - 28f_{j-1} - f_{j-2}) \\ \vdots \\ \frac{1}{2dy}(-f_{N-2} + f_N) \\ 0.0 \end{bmatrix}, \quad (24)$$

$$\begin{bmatrix} 1 & & & & & & \\ & 1 & & & & & \\ & \ddots & \ddots & \ddots & & & \\ & & 1 & 3 & 1 & & \\ & & & \ddots & \ddots & \ddots & \\ & & & & & 1 & \\ & & & & & & 1 \end{bmatrix} \begin{bmatrix} f'_0 \\ f'_1 \\ \vdots \\ f'_j \\ \vdots \\ f'_{N-1} \\ f'_N \end{bmatrix} = \begin{bmatrix} \frac{1}{2dy^2}(-7f_0 + 8f_1 - f_2) \\ \frac{1}{2dy^2}(f_0 - 2f_1 + f_2) \\ \vdots \\ \frac{1}{4dy^2}(3f_{j-2} + 48f_{j-1} - 102f_j + 48f_{j+1} + 3f_{j+2}) \\ \vdots \\ \frac{1}{2dy^2}(f_{N-2} - 2f_{N-1} + f_N) \\ \frac{1}{2dy^2}(-7f_{N-2} + 8f_{N-1} - f_N) \end{bmatrix}. \quad (25)$$

Table 1 shows the round-off error for the first derivatives schemes and the stencil size of 2^{nd} order explicit and 6^{th} order compact methods:

Schemes	Max L.H.S. Stencil Size	Max R.H.S. Stencil Size	Truncation Error
2^{nd} order - 1st derivatives	1	3	$-\frac{1}{6}h^2f^4$
2^{nd} order - 2nd derivatives	1	3	$-\frac{1}{12}h^2f^4$
6^{th} order compact - 1st derivatives	3	5	$\frac{1}{28}h^6f^7$
6^{th} order compact - 2nd derivatives	3	5	$-\frac{1}{2414}h^6f^8$

Table 1: Stencil size and round-off error.

The non-linear terms in Navier-Stokes equation can produce an numerical instability adding disturbances non physical of high frequency in the variables during the simulation. In order to remove a short length scales

a high-order compact filter was implemented in agreement with Lele, 1992. The numerical filter was applied in the last step of Runge-Kutta scheme. This filter consist in to recalculate the distribution of primitive variables through one 4^{th} compact scheme. These schemes can be solved through one pentadiagonal system as follow below

$$\begin{bmatrix} 1 & \alpha & \beta & & & & & \alpha & \beta \\ \beta & 1 & \alpha & \beta & & & & & \alpha \\ \alpha & \beta & 1 & \alpha & \beta & & & & \\ & \ddots & \ddots & \ddots & \ddots & \ddots & & & \\ & & \alpha & \beta & 1 & \alpha & \beta & & \\ & & & \ddots & \ddots & \ddots & \ddots & \ddots & \\ & & & & \alpha & \beta & 1 & \beta & \alpha \\ \alpha & & & & & \alpha & \beta & 1 & \beta \\ \beta & \alpha & & & & & \alpha & \beta & 1 \end{bmatrix} \begin{bmatrix} \widehat{f}_0 \\ \widehat{f}_1 \\ \widehat{f}_2 \\ \vdots \\ \widehat{f}_i \\ \vdots \\ \widehat{f}_{N-2} \\ \widehat{f}_{N-1} \\ \widehat{f}_N \end{bmatrix} = \tag{26}$$

$$\begin{bmatrix} \frac{d}{2}f_{N-3} + \frac{c}{2}f_{N-2} + \frac{b}{2}f_{N-1} + af_0 + \frac{b}{2}f_1 + \frac{c}{2}f_2 + \frac{d}{2}f_3 \\ \frac{d}{2}f_{N-2} + \frac{c}{2}f_{N-1} + \frac{b}{2}f_0 + af_1 + \frac{b}{2}f_2 + \frac{c}{2}f_3 + \frac{d}{2}f_4 \\ \frac{d}{2}f_{N-1} + \frac{c}{2}f_0 + \frac{b}{2}f_1 + af_2 + \frac{b}{2}f_3 + \frac{c}{2}f_4 + \frac{d}{2}f_5 \\ \vdots \\ \frac{d}{2}f_{i-3} + \frac{c}{2}f_{i-2} + \frac{b}{2}f_{i-1} + af_i + \frac{b}{2}f_{i+1} + \frac{c}{2}f_{i+2} + \frac{d}{2}f_{i+3} \\ \vdots \\ \frac{d}{2}f_{N-5} + \frac{c}{2}f_{N-4} + \frac{b}{2}f_{N-3} + af_{N-2} + \frac{b}{2}f_{N-1} + \frac{c}{2}f_0 + \frac{d}{2}f_1 \\ \frac{d}{2}f_{N-4} + \frac{c}{2}f_{N-3} + \frac{b}{2}f_{N-2} + af_{N-1} + \frac{b}{2}f_0 + \frac{c}{2}f_1 + \frac{d}{2}f_2 \\ \frac{d}{2}f_{N-3} + \frac{c}{2}f_{N-2} + \frac{b}{2}f_{N-1} + af_0 + \frac{b}{2}f_1 + \frac{c}{2}f_2 + \frac{d}{2}f_3 \end{bmatrix}, \tag{27}$$

where the coefficients of the system are given by

$$\alpha = 0.6522474,\ \beta = 0.1702929,\ a = 0.9891856,\ b = 1.3211800,\ c = 0.3333548,\ d = 0.001359850.$$

Implementation of the filtering schemes on domains with non-periodic boundaries requires the near boundary nodes to be treated separately. Therefore explicit near boundary formulas are

$$\widehat{f}_1 = \frac{15}{16}f_1 + \frac{1}{16}(4f_2 - 6f_3 + 4f_4 - f_5) \tag{28}$$

$$\widehat{f}_2 = \frac{3}{4}f_2 + \frac{1}{16}(f_1 + 6f_3 - 4f_4 + f_5) \tag{29}$$

$$\widehat{f}_3 = \frac{5}{8}f_3 + \frac{1}{16}(-f_1 + 4f_2 + 4f_4 - f_5) \tag{30}$$

The truncation error for these methods is shown in table below

Schemes	Max L.H.S. Stencil Size	Max R.H.S. Stencil Size	Truncation Error
27	5	7	$-\frac{1}{228}h^4f^4$
28	1	5	$\frac{3}{48}h^4f^4$
29	1	5	$\frac{11}{192}h^4f^4$
30	1	5	$-\frac{3}{48}h^4f^4$

Table 2: Stencil size and round-off error for numerical filter.

Time-advance of the computational variables (ρ,ρu_i,E_t) is obtained by the 4^{th} order Runge-Kutta method. The discretized transport equations are used to determine the values of the variables at each point of the computational domain at time $t_{n+1} = t_n + dt$. The schemes here described works in 4 steps (Ferziger and Peric, 1997). The first two steps use a formulation of Euler "predictor" explicit and a formulation of Euler "corrector" implicit for the same time $t + dt/2$. The following step is a "predictor" based on the rule of the medium point for the whole step $(t + dt)$ and the last, "corrector" is based on Simpson's rule. The combination of these steps results in a 4^{th} order accuracy algorithm.

3.4. Grid Stretching

The classical governing equations of fluid dynamics have been presented in section 3. These equations have been written in either vector or tensor form. These equations can be expressed in terms of any generalized orthogonal coordinate system. For many applications, a orthogonal coordinate system is desirable such as a shear layer problem. In this section, we will show how the governing equations can be transformed from a Cartesian coordinate system to any general orthogonal coordinate system. In this process, we will demonstrate how simple transformations can be used to cluster grid points in regions of large gradients and how to transform a non-rectangular computational region in the physical plane into a rectangular uniformly-spaced grid in the computational plane.

Flow-field has to precisely gridded because important variations of velocity and temperature are observed in this field. Therefore we would like to simulate some fields with axes y between $-Ly/2.0$ and $Ly/2.0$. In the points near free stream the field requires a resolution with less accuracy, while in the interior of the domain we need greater resolution. It is possible to realize a stretching of the grid to decrease number of points required.

In this work we use a formula coming from Anderson *et al.*, 1984 giving a constant stretching, with β, which is a stretching parameter and y_c, the locations, where this stretching is centered.

$$y = D\left\{1 + \frac{\sinh[\beta(\eta - A)]}{\sinh(\beta A)}\right\} \tag{31}$$

where

$$A = \frac{1}{2\beta}\ln\left[\frac{1 + (e^{\beta} - 1)(y_c/H)}{1 + (e^{-\beta} - 1)(y_c/H)}\right] \tag{32}$$

In order to apply this transformation to the governing equations, the following partial derivatives are formed. For the first derivatives we have the following simple relation

$$\frac{\partial f}{\partial y} = \frac{\partial f}{\partial \eta}\frac{\partial \eta}{\partial y} \tag{33}$$

where

$$\frac{\partial \eta}{\partial y} = \frac{\sinh(\beta A)}{\beta D\sqrt{1 + [(y/D) - 1]^2\sinh(\beta A)^2}} \tag{34}$$

This relation should be used with high-order compact schemes. Applying the relation 33 for derivatives approximations, we are obtained the following tridiagonal compact schemes for first derivatives

$$\alpha\psi'_{j-1}\left.\frac{\partial f}{\partial y}\right|_{j-1} + \psi'_j\left.\frac{\partial f}{\partial y}\right|_{j} + \alpha\psi'_{j+1}\left.\frac{\partial f}{\partial y}\right|_{j+1} = a\frac{f_{i+1} - f_{i-1}}{\delta\eta} + b\frac{f_{i+2} - f_{i-2}}{\delta\eta} \tag{35}$$

where $\psi'_j = \frac{1}{\partial\eta/\partial y}$.
The same procedure can be applied for the second derivatives

$$\frac{\partial^2 f}{\partial y^2} = \frac{\partial^2 \eta}{\partial y^2}\frac{\partial f}{\partial \eta} + \left(\frac{\partial \eta}{\partial y}\right)^2\frac{\partial^2 f}{\partial \eta^2} \tag{36}$$

where

$$\frac{\partial^2 \eta}{\partial y^2} = -\frac{\sinh(\beta A)^3(y/D - 1)}{[\beta D^2\sqrt{1 + [(y/D) - 1]^2\sinh(\beta A)^2}]^{\frac{3}{2}}} \tag{37}$$

Equation 36 can be rewritten as

$$\frac{\partial^2 f}{\partial \eta^2} = \frac{1}{\psi'^2}\frac{\partial^2 f}{\partial y^2} - \left[\frac{\psi''}{\psi'^2}\frac{\partial f}{\partial \eta}\right] \tag{38}$$

Using the relation $\frac{\psi''}{\psi'^2}\frac{\partial f}{\partial \eta} = \frac{\psi''}{\psi'^3}\frac{\partial f}{\partial y}$ and replacing the term in square brackets between hook in equation 38 we have

$$\frac{\partial^2 f}{\partial \eta^2} = \frac{1}{\psi'^2}\frac{\partial^2 f}{\partial y^2} - \frac{\psi''}{\psi'^3}\frac{\partial f}{\partial y} \tag{39}$$

Therefore, applying the relation 39 to the second derivative approximation we have the tridiagonal system as follow below

$$\alpha \frac{1}{\psi'^2_{j-1}} \frac{\partial^2 f}{\partial y^2}\bigg|_{j-1} + \frac{1}{\psi'^2_j} \frac{\partial^2 f}{\partial y^2}\bigg|_j + \alpha \frac{1}{\psi'^2_{j+1}} \frac{\partial^2 f}{\partial y^2}\bigg|_{j+1} = a\frac{f_{i+1} - f_{i-1}}{\delta\eta} + b\frac{f_{i+2} - f_{i-2}}{\delta\eta} + \frac{\psi''}{\psi'^3}\frac{\partial f}{\partial y} \tag{40}$$

Bogey *et al.*, 2000 recommend that the grid stretching should not exceed 1.8% in order to avoid problems with space derivatives. Another assumption of these methods is that the mesh must be sufficiently smooth so that $\partial y/\partial\eta$ and $\partial^2 y/\partial\eta^2$ can be defined, and, in practice, calculated without appreciable loss in the overall accuracy. For this simulation $\beta = 12$ was assumed. Other tests was performed with this parameter and this value showed the best results. With $\beta = 15$ the code presents a numerical instabilities in the time integration. These results will be discussed in the next sections.

4. Numerical Results

In this section, results from direct numerical simulations of the compressible Navier-Stokes equations are used to show the physics of the vorticity transport phenomenon in the linear and non-linear regime of the time-developing mixing layer problem. Firstly, an analysis of the amplification rate in the linear regime was performed to compared the growth rate obtained numerically with other theoretical results. These validation tests were extended to a regime governed by non-linear. First, it was simulated a flow using a small disturbance of a stipulated mode. In this case, it was possible to reproduce the vorticity phenomenon in streamwise direction. After, a subharmonic mode was introduced in the disturbance flow to develop the pairing that corresponding to the secondary instability. According to these studies was possible to confirm the strong reduction in shear layer growth rate as Mach number is increased. In all simulations here a non-uniform grid was used to reproduce the phenomenon, and consequently, an analysis of the efficacy of grid stretching was performed in these studies.

In these numerical investigations a relatively high Reynolds number was chosen to ensure that the viscous effects were small. The high Mach number was select to analyze the effects of compressibility in the evolution of two-dimensional disturbances. Moreover, a high-order compact finite-difference scheme was used to solve spatial derivatives. Time-advance of the computational primitives variables were obtained by a 4^{th} order explicit Runge-Kutta scheme. In x-direction, periodic boundary conditions were utilized, while in y-direction a free-slip condition was used. In order to remove short length scales, a 4^{th} order compact numerical filter was applied in x- and y-directions. The analysis of the filter implementation is show in the technical report given by Germanos and Medeiros, 2005.

4.1. Linear Stability

This section presents the evolution of two-dimensional sinusoidal disturbances in a free shear layer problem for the tangent hyperbolic profile in the regime governed by linear theory. The objective of this simulation was to compare the growth rate of the two-dimensional disturbances with other works. Theoretical results used in this paper were obtained through the temporal linear stability analysis carried out by Sandham and Reynolds, 1991. Here, simulations were performed to verify the effect of Mach number in the evolution of instabilities. These results confirm the prediction of linear stability theory that at low Mach numbers the two-dimensional instability waves are the most unstable.

An important aspect to be considered in these simulations is the treatment of the vertical diffusion. This diffusion increases the width of the free shear layer during the simulation, which implies a variation of the mean flow over time. Thus, there should be a variation of the amplification rate, even in the linear regime. The strategy adopted here to avoid this diffusion was to cancel the vertical diffusions terms for the base flow.

First the problem was simulated with Euler equations. In this case, the convective Mach number selected were 0.4 and 0.8. The mesh for these problems has a dimension of 40×80, that corresponds to the number of points in $x-$ and $y-$ directions. The grid spacing used in the simulation with a uniform mesh was $dx = 0.41$ and $dy = 0.30$, respectively, grid spacing in longitudinal and normal direction. In the non-uniform mesh in y-direction the minimum and maximum mesh spacing was $dy_{min} = 0.0089$ and $dy_{max} = 1.67$. The mesh spacing is constant in x-direction. Moreover, the initial amplitude of the disturbance was approximately 10^{-6}. This amplitude ensure that the phenomenon will start in regime governed by linear theory. The time step dt of this simulation was 10^{-3}. These tests were performed using a disturbance with only one mode. The wavenumber α of this disturbance was $\alpha_1 = 0.75$. This is close to the wavenumber of maximum amplification.

Figure 1 shows the growth rate of unstable waves at convective Mach number equals to 0.4 as a function of non-dimensional time. In this figure the vertical coordinate is in logarithm scale. The dashed-dotted line is the numerical result for a uniform grid. The amplification rate obtained from this line is about 0.27. The disagreement could be attributed to the numerical order generate by constant spacing grid used in these simulations.

The solid line shows the result for a non-uniform grid with a stretching parameter of $\beta = 12$. The growth rate in this line corresponds to an amplification rate of 0.30 which is in agreement with theoretical results.

Figure 2 presents the amplification rate at convective Mach number $M_c = 0.8$. Similar to the previous results, the dashed-dotted line gives an amplification rate of about 0.17 for uniform grid. The theoretical results for this convective Mach number shows a amplification rate about of 0.14. The solid line represents the same results with the use of a grid stretching. The growth rate obtained in this simulation was 0.15. This result is very close to the prediction. Based on these results we can observe that the amplification rate obtained in these simulations was significantly reduced with increasing of convective Mach number. These results confirm the reduction in the amplification rate for high Mach numbers. Therefore the agreement of these results is remarkable.

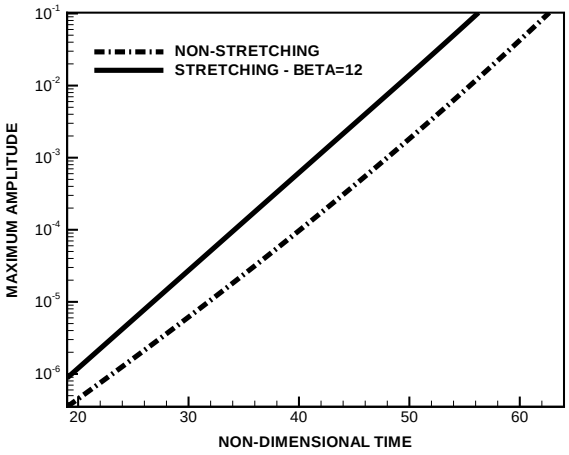

Figure 1: Amplitude evolution from inviscid flow at Mach number equals to 0.4 and wavenumber approximately to 0.75.

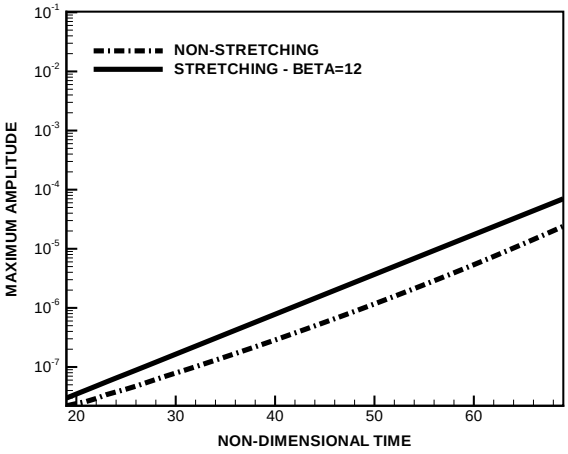

Figure 2: Amplitude evolution from inviscid flow at convective Mach number equals to 0.8 and wavenumber approximately to 0.75.

In the following, simulations for the compressible Navier-Stokes equations were performed. The initial amplitude of the disturbance of the dominant mode was the same as in previous simulations. The wavenumber of the disturbance selected for the simulations was $\alpha = 0.82$. This growth rate was chosen to compare the results with theoretical results. In figure 3 the dashed-dotted line show the time evolution of two-dimensional disturbance at convective Mach number equals 0.4 for a grid with constant spacing. The amplification rate obtained in these results is about 0.26. This is a underestimate rate compared to theoretical results that gives a amplification rate about 0.28. The solid line show a growth rate approximately of 0.29 with the use of grid stretching. Although these results be overestimate in relation to the theory, it is closed to the linear analysis. These results confirm that the simulations with grid stretching lead to improved amplification rate obtained numerically.

Figure 4 shows the time evolution for convective Mach number equals to 0.8 and Reynolds number equals to 500. The same analysis was made. The amplification rate generate for a uniform mesh was 0.14, while for a mesh with stretching the rate was approximately 0.13. Both results are close to the analytical results where gives a grow rate about 0.11. Furthermore, we can realize that using of grid stretching improved the agreement in the analysis of amplification rate. Emphasizes that the same number of points in y-direction was used to simulate the phenomenon with an uniform and non-uniform mesh. Therefore, the grid stretching significantly improves the accuracy for a number of grid points. Alternatively, the same numerical accuracy can be achieved with fewer grid points by clustering the points in the region of interest thus reducing computational cost.

4.2. Non-linear Stability

For the a numerical investigations discussed here, the full compressible Navier-Stokes equations were considered to analyze the problem in the non-linear regime. The evolution of a small two-dimensional disturbance in shear layer was performed in a non-uniform grid. This grid allows fro greater resolution in the interior of the computational domain where the instability phenomenon occurs. Consequently, the numerical error in this zone is reduced due to the refinement of the grid. Another aspect considered here is that the grid is stretched in zones close to the boundaries where the instabilities waves have decayed. In order to verify the code, simu-

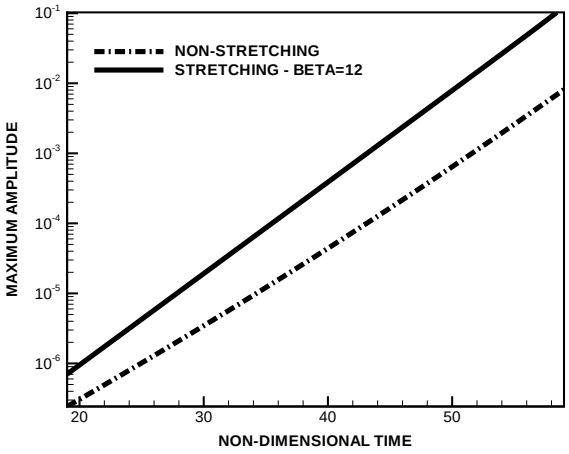

Figure 3: Amplitude evolution from inviscid flow at convective Mach number equals to 0.4 and wavenumber approximately to 0.75.

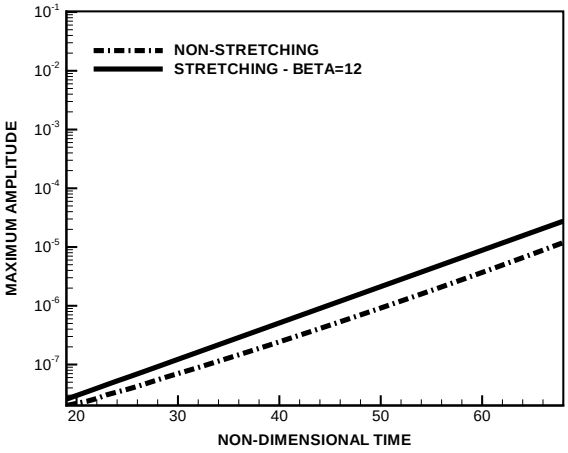

Figure 4: Amplitude evolution from inviscid flow at convective Mach number equals to 0.8 and wavenumber approximately to 0.75.

lations were carried out to reproduce the secondary instability mechanism. According to the theory a pairing phenomenon produces waves that propagate towards the boundaries. These waves can be reflected from the boundaries resulting in a non-physical distortion of the numerical results. The grid stretching can prevent that these waves reaches the boundaries, rendering the code more stable in time-advancement.

As a first step, the simulation of the compressible Euler equations for a two-dimensional flow was performed. The objective here is to determine the maximum allowable grid stretching for which the computational remains stable. For this problem a mesh with a dimension of 40×80, number of points in x- and y-direction was chosen. The grid spacing used in this simulation for a uniform mesh was $dx = 0.50$ and $dy = 0.30$, respectively, grid spacing in longitudinal and normal direction. For non-uniform grid the minimum and maximum spacing in y-direction was $dy_{min} = 0.0089$ and $dy_{max} = 1.67$. Mesh spacing is constant in the x-direction. The initial amplitude of the disturbance was approximately 10^{-6}. This value satisfies the CFL condition. The wavenumber of the disturbance selected for the simulation was $\alpha_1 = 0.75$ for dominant mode and $\alpha_2 = \alpha_1/2$ for the subharmonic mode. This is close to the wavenumber of maximum amplification. Figure 5 show the non-linear evolution of the disturbances in time for a uniform mesh. In this figure, the coordinate z presents the vorticity component in the x-direction. It can be observed that the shear region produces waves that propagate towards the free stream boundaries. This production of sound waves is undesirable and has to be minimized.

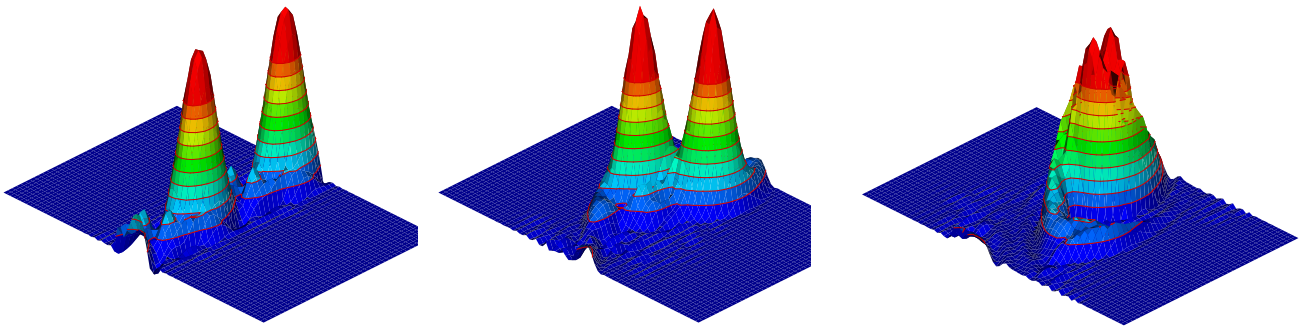

Figure 5: Amplitude evolution from inviscid flow at convective Mach number equals to 0.4 and wavenumber approximately to 0.89. The subharmonic mode was introduced here to reproduce the secondary instability. A uniform grid in the y-direction was used in these simulations. The frames presented correspond to the non-dimensional times 60, 68 and 78.

Figure 6 shows the evolution of the same problem on a non-uniform grid. Different from the stretching parameter used for the linear regime, the stretching parameter chosen for the non-linear regime was $\beta = 10$. Many values for this parameter have been tested and this value presents the best results in relation computational efficiency, without causing numerical problems with the spatial derivatives. It can be seen in this figure that the formation of sound waves in the shear zone was strongly reduced with the application of stretching. In figure 7 we can seen a simulation with the application of $\beta = 15$. In this case, the numerical scheme becomes unstable in time. These results confirm that the grid stretching cannot exceed 1.8% of the maximum grid lengths.

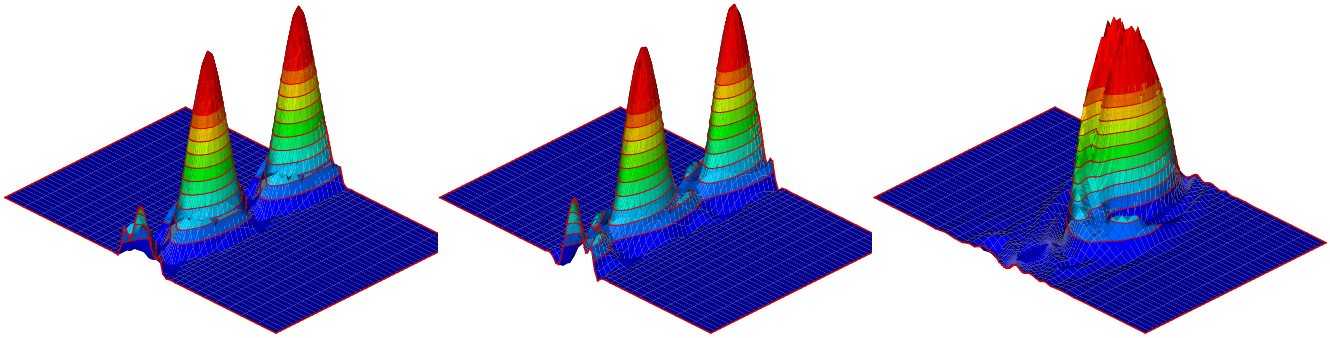

Figure 6: Amplitude evolution from inviscid flow at convective Mach number equals to 0.4 and wavenumber approximately to 0.89 for a non-uniform grid. The disturbance here was composed of a fundamental and subharmonic mode. A non-uniform grid in y-direction was used in these simulations and the stretching parameter was selected by $\beta = 12$. The frames presented correspond to the non-dimensional times 60, 68 and 96.

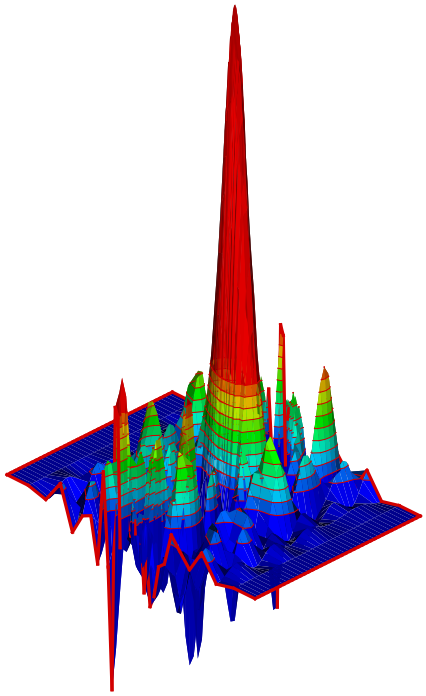

Figure 7: Amplitude evolution from inviscid flow at convective Mach number equals to 0.4 and wavenumber approximately to 0.89 for a non-uniform grid. The disturbance here was composed of a fundamental and subharmonic mode. A non-uniform grid in y-direction was used in this simulations and the stretching parameter was selected as $\beta = 15$. The frame presented corresponds to the non-dimensional time of 96.

More tests were performed for the evolution of non-linear instabilities. Here the non-linear tests were carried out to verify the code when the disturbances have reached large amplitudes. In this case, the non-linear effects

need to be considered. The theory associated with these effects is more complex than for small-amplitude, linear disturbances and will not be present here. Previews of the subject can be found in Herbert, 1988 and Medeiros, 2000. The summary of the main results, given below, is enough for carrying out the tests proposed. Both theory and experiment show that in a shear layer the disturbance does not grow to infinity. Instead this disturbance satures in a limit cycle pattern of co-rotating vortices. In turn, the vortices are themselves unstable to a subharmonic disturbance. It means that if a subharmonic oscillation exists in the flow this oscillation will grow. The result is a pairing of vortices. It is important to emphasize that in the system there is no mechanism for the production of subharmonic disturbances, but only for amplification. In the numerical solution of the equations of motion, this seeding of subharmonic waves may come from round-off error. The growth of subharmonic provides a good indication of the numerical error of CFD codes.

The simulations performed for this analysis employ the full compressible Navier-Stokes equations, including the viscous terms. The initial disturbance amplitude of the dominant and subharmonic mode was the same that in the previous studies. First, the disturbance was composed of only one mode with wavenumber $\alpha = \pi/4$. Figure 8 shows a sequence of the evolution of two-dimensional disturbances over time. Initially in the linear regime, the disturbance is very small and display a sinusoidal pattern. The fundamental mode grows and two satures vortices are formed, which corresponds to the limit cycle oscillation. The vortices dissipate due to viscous effects. Under these circumstances the non-linear theory predicts no pairing. Although there are no tendency of pairing, but at very late times a pairing occurs. Figure 9 shows, that indeed, the vortices take a rather long time to pair. It occurred only when the vortices were almost entirely dissipated by viscous effects. Since the subharmonic excitation was not excited, the explanation for this behavior is that the subharmonic seed for the pairing must have arisen from numerical error.

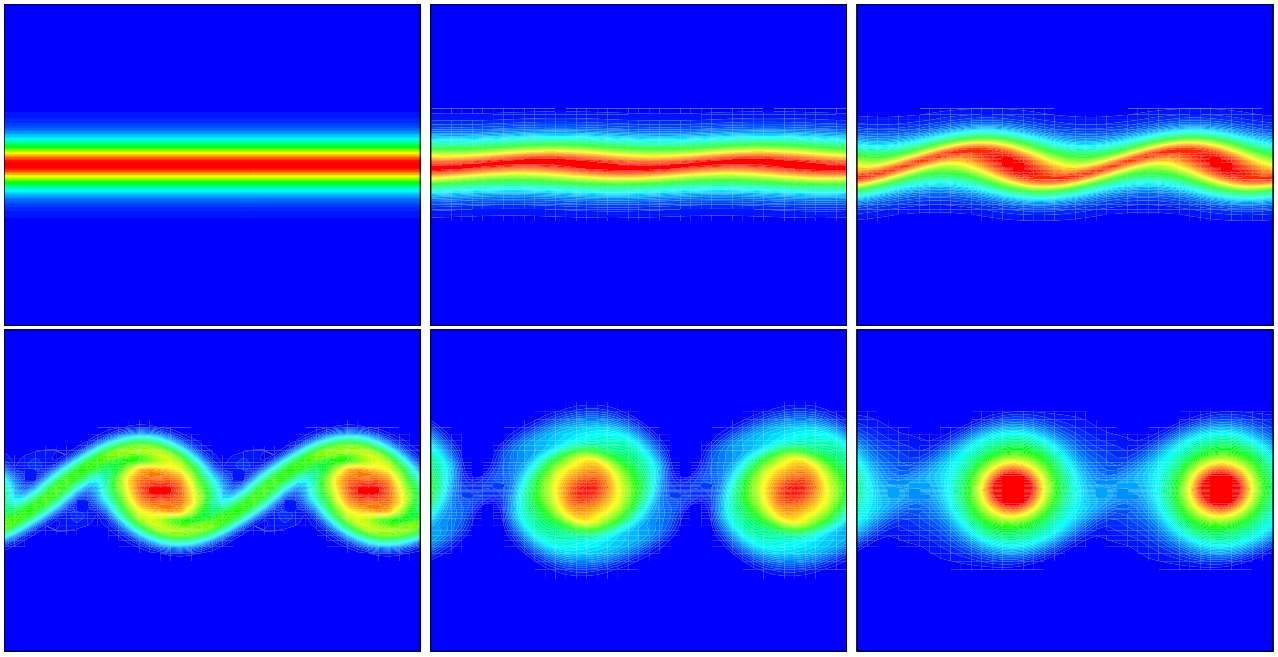

Figure 8: The linear and nonlinear two-dimensional evolution of disturbance composed of a dominant mode. A non-uniform grid in y-direction was used in these simulations. The frames presented correspond to the non-dimensional times 10, 55, 60, 65, 75 and 100

The following simulations were performed with the deliberate introduction of a subharmonic perturbations. The wavenumber of the disturbance selected for the simulation was $\alpha_1 = 0.82$ for fundamental mode, and $\alpha_2 = \alpha_1/2$ for the subharmonic mode. The characteristics of the flow in first stages were identical to the previous test. In this case the same behavior can be seen in figure 10. In the initially stage a sinusoidal growth was displayed. After the fundamental mode arises and saturates, the subharmonic mode grows and two of the primary structures begin to rotate around each other. After, the pairing occurs between these two vortices and one large vortex results. In this case, the pairing occurs due a excited subharmonic disturbance rather than numerical error. As result that the pairing occurs in earlier non-dimensional time of approximately 105. In the previous simulation the same phenomenon occurs for non-dimensional time approximately 200. These results indicate that the secondary instability was trigged by growing of the numerical error, which was very small compared to the amplitude of the perturbations introduced.

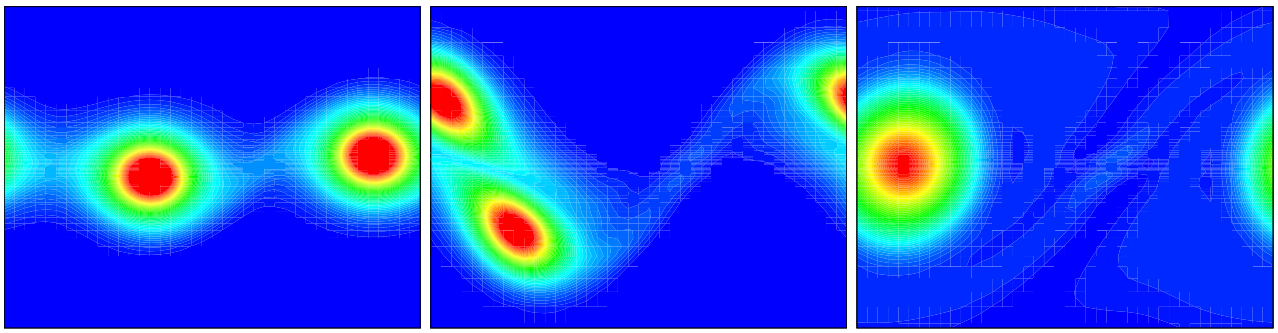

Figure 9: The linear and nonlinear two-dimensional evolution of disturbance composed of a dominant mode. A non-uniform grid in y-direction was used in these simulations. The frames presented correspond to the non-dimensional times 140, 150 and 200

Results for convective Mach number equals to 0.6 are shown in sequence 11. The first frame shows the flow at non-dimensional time equals to 55. Here the two-dimensional disturbances excited by the fundamental mode is not evident. At the same time, it can be observed in the sequence of $M_c = 0.4$ that the flow presents a sinusoidal pattern. In order words, at this stage the disturbance at $M_c = 0.4$ grows faster than the disturbance at $M_c = 0.6$. Proceeding with this analysis at $M_c = 0.6$, it can be observed in the second frame that the fundamental mode grows becoming more clear for non-dimensional time equals to 73. The next frame presents the structures of co-rotating vortices before a merger at time about 85. The previous results at $M_c = 0.4$ show the same phenomenon at an earlier time of 65. Later the disturbance excited by the subharmonic perturbation become evident leading to the pairing which occurs at time of 117. At $M_c = 0.4$ the same phenomenon occurred at a time of about 100. According to these studies we can conclude that the amplification rate is strongly reduced as the convective Mach number is increased.

This analysis was extended to the case of a convective Mach number of 0.8 where compressibility effects become important, as shown in figure 12. An interesting behavior can be observed in this sequence. First we can seen that the growth rate of two-dimensional waves is strongly reduced with the convective Mach number is increased. According to this sequence we can realize that the fundamental mode grows and are displayed with more clear at non-dimensional time of 115. This delay correspond a 52% of time that occurs the same behavior at convective Mach number of 0.4. Once again the amplification rate was reduced at high convective Mach numbers in accordance with theory. Another aspect can be analyzed for this simulation. The plots of vorticity show a clear change in structure as the convective Mach number is raised. The vortices become very elongated in the streamwise direction at convective Mach number of 0.8. A physical explanation of the shape change will now be suggested. A fluid element approaching the structure from the upper left-hand-side experiences an expanding flow, and a reduction in vorticity, until it is alongside the vortex. Then the element is subject to a compression, with an associated increase in vorticity as it approaches the trailing edge of the vortex, and the stagnation region behind. A similar process affects fluid elements approaching from the lower right-hand-side. The overall effect is that vorticity above and below the vortex is reduced, and vorticity in front and behind the vortex is increased, leading to a structure elongated in the streamwise direction. The elongated vortex does not wrap any new fluid around the structure, and it cannot then be engulfed and mixed, and there is only growth by viscous diffusion. The circular vortex wraps fluid from the free streams around itself, and grows strongly. If we assume a monotonic trend we see that the effect of an elongated vortex is to reduce the growth rate of the shear layer.

5. Conclusions

In this work the numerical simulation of a compressible free shear layer was performed. The governing equations were the compressible Navier-Stokes equations. A 6^{th} order compact finite-difference scheme was used for discretizing the spatial derivatives. In order to remove a short length scales, a $4th$ order compact filter was implemented. The method adopted was time accurate, using a 4^{th} order Runge-Kutta scheme. A free-slip boundary condition was used in y-direction. As well as a exponential decay condition in y-direction. Periodic boundary condition was implemented in x-direction. Lastly, these simulations were carried out on a

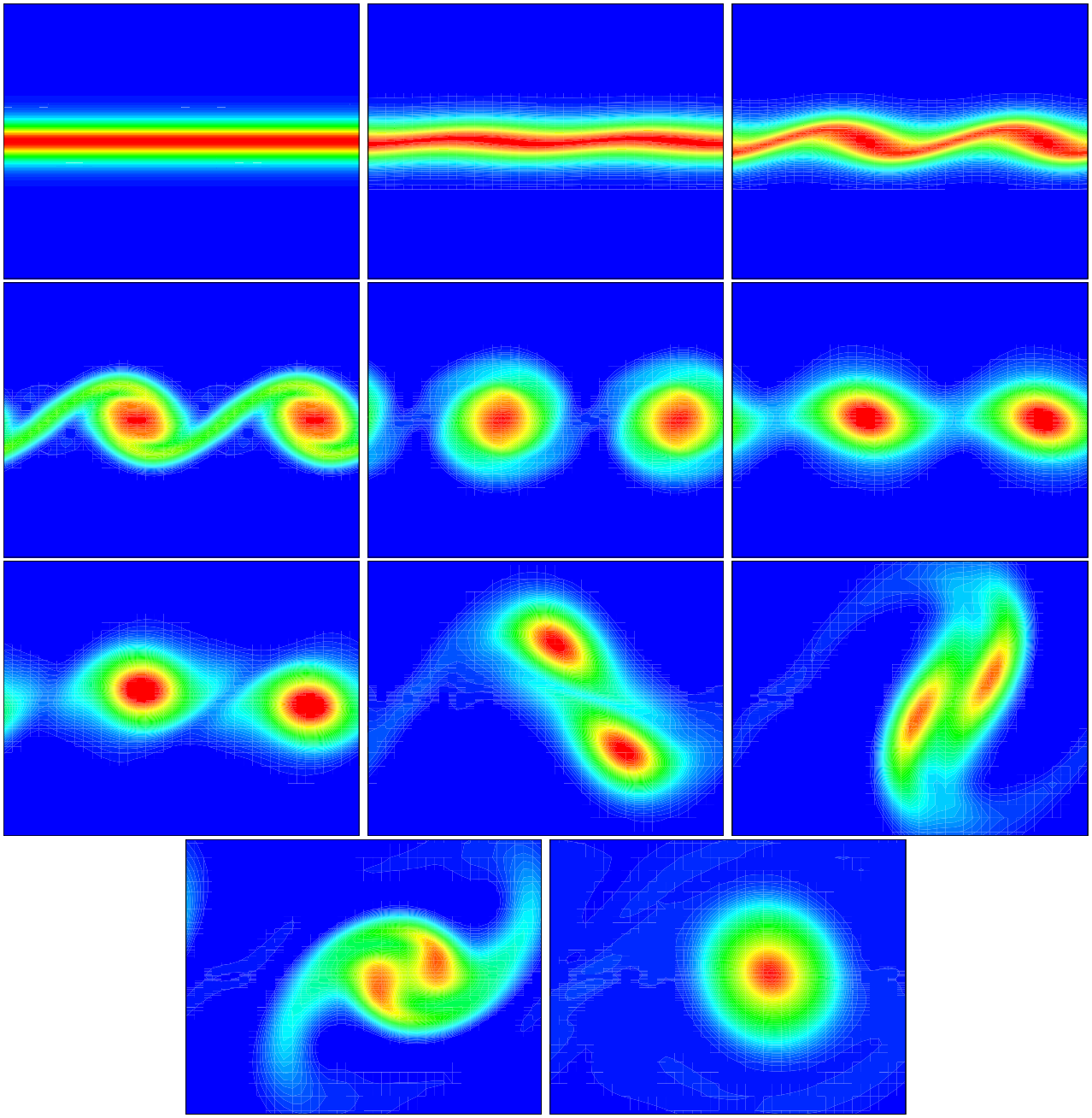

Figure 10: The linear and nonlinear two-dimensional evolution of disturbance composed of a dominant mode and a subharmonic mode at convective Mach number equals to 0.4. A non-uniform grid in y-direction was used in these simulations. The frames presented correspond to the non-dimensional times 30, 55, 60, 65, 70, 80, 90, 100, 105, 110 and 165.

non-uniform grid. This technique was utilized to remove sound waves produced by the pairing that occurs due a secondary instability. These waves can propagate in normal direction forwards free stream boundaries and might be reflected back contaminating the numerical solution.

The compressible shear layer flow was simulated giving some interesting results. In the linear regime was possible to obtain an good amplification rate with the use of stretching in y-direction. This non-uniform grid allows for a high resolution in the interior of the domain. The growth rate for uniform and non-uniform grids was analyzed and the cases with a grid stretching show the best results. Also, the effect of the convective Mach number on the growth rate of two-dimensional disturbances was analysis. The results confirm a reduction in the growth rate for high convective Mach numbers as also predicted linear theory stability.

For simulations in the non-linear regime the results were very interesting and it was possible reproduce some

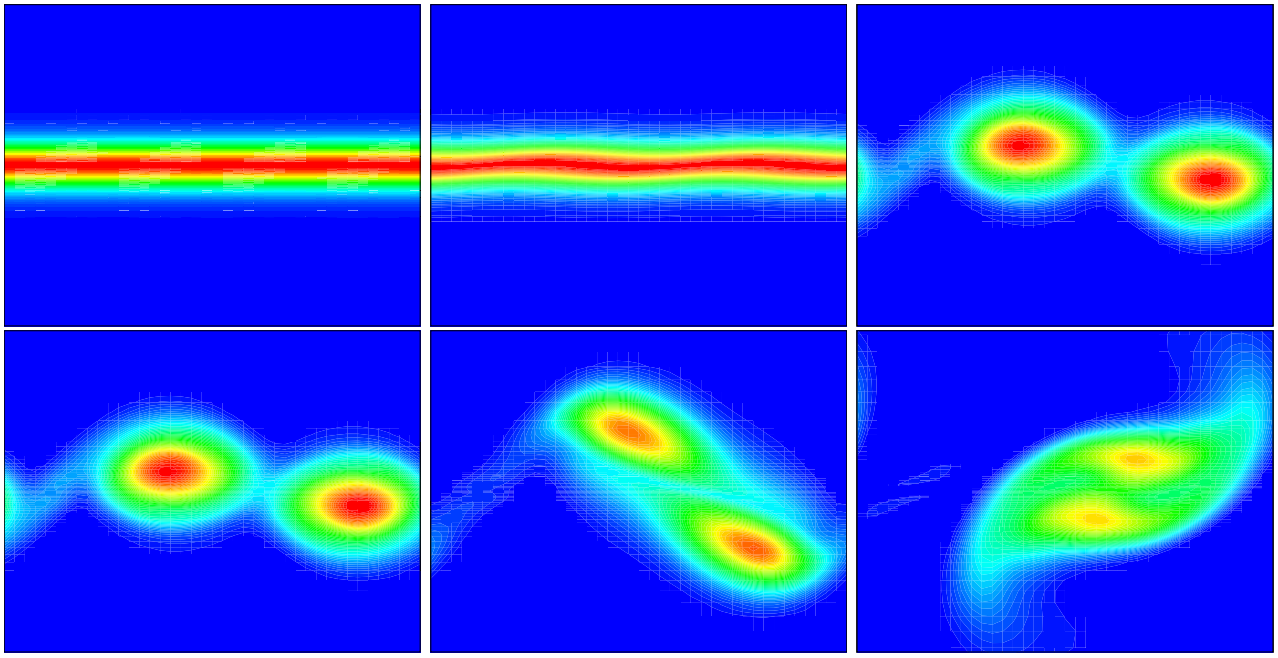

Figure 11: The linear and nonlinear two-dimensional evolution of disturbance composed of a dominant and a subharmonic mode at convective Mach number equals to 0.6. A non-uniform grid in y-direction was used in these simulations. The frames presented correspond to the non-dimensional times 55, 73, 85, 110, 117 and 128.

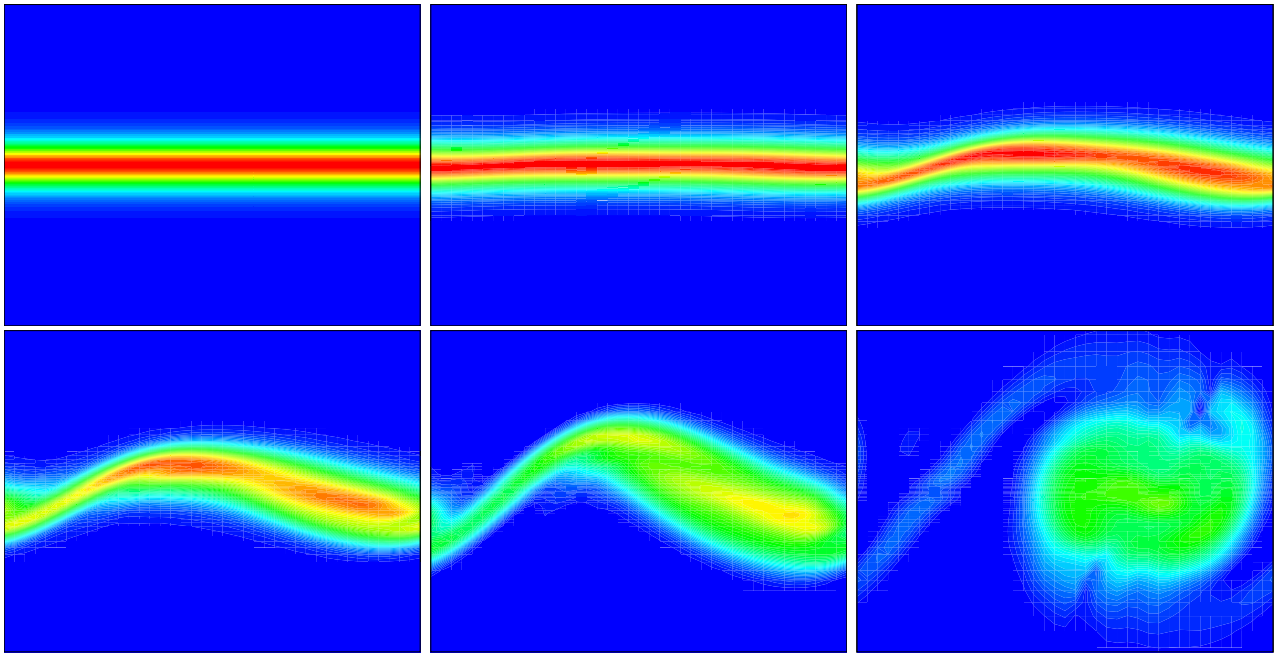

Figure 12: Linear and nonlinear two-dimensional evolution of disturbances composed of a fundamental mode and a subharmonic mode at convective Mach number equal 0.8. A non-uniform grid in y-direction was used in these simulations. The frames presented correspond to the non-dimensional times 30, 115, 125, 133, 160 and 170.

important physical phenomena. First, the effects of the grid stretching was analyzed. Test was performed to verify the efficiency of grid stretching in damping at undesirable sound waves produced by the shear zone. In this analysis we observed that these waves were strongly reduced in the direction towards the boundaries, if grid stretching was applied.

Following the evolution of disturbances composed of a dominant mode were presented. In these simulations

the two-dimensional disturbances show a sinusoidal pattern and structure of vortices forming until the limit cycle oscillation. Lastly it was introduced a subharmonic mode, and this way, it was possible to reproduced the secondary instability. In this case, a pairing occurs between the two vortices and one large vortice results. From these results it was possible to verify the effect of the convective Mach number on the amplification rate of two-dimensional waves. These results confirm that the growth rate were strongly reduced as the Mach number was increased. This behavior is in agreement with other studies of hydrodynamic instability in compressible shear layers and the authors of this work concluded that the results for all cases were very good.

6. Acknowledgments

The financial support from FAPESP (State of São Paulo Research Support Foundation) – Grant number 02/09256-3 is greatly acknowledged.

7. References

Anderson, D. A., Tannehill, J. C., and Pletcher, R. H., 1984, "Computational Fluids Mechanics and Heat Tranfer", Hemisphere Publishing Corporation.

Bernal, L. and Roshko, A., 1986, Streamwise vortex structure in plane mixing, "J. Fluid Mech.", Vol. 170, pp. 429–525.

Birch, S. F. and Eggers, J. M., 1973, A critical review of the experimental data for developed free turbulent shear layers., "NASA SP", Vol. 321, pp. 11–40.

Blumen, W., Drazin, P. G., and Billings, D. F., 1975, Shear Layer instability of an inviscid compressible fluid. Part 2, "J. Fluid Mech.", Vol. 71, pp. 305–316.

Bogey, C., Bailly, C., and Juve, D., 2000, Numerical Simulation of Sound Generated by Vortex Pairing in a Mixing Layer., "AIAA Journal", Vol. 38, pp. 2210–2218.

Brown, G. L. and Roshko, A., 1974, On density Effects and Large Structure in Turbulent Mixing Layer, "J. Fluid Mech.", Vol. 64, pp. 775–816.

Canuto, C., Hussaini, M. Y., Quarteroni, A., and Zang, T. A., 1987, "Spectral Methods in Fluid Dynamics".

Collatz, L., 1966, "The numerical treatment of differential equations", Springer-Verlag, New York.

Colonius, T., Lele, S. K., and P., M., 1997, Sound generation in a mixing layer, "J. Fluid Mech.", Vol. 330, pp. 375–409.

Eibler, W. and Bestek, H., 1996, Spatial Numerical Simulations of Linear and Weakly Nolinear Wave Instabilities in Supersonic Boundary Layers, "Theoretical and Computational Fluid Dynamics", Vol. 8, pp. 219–235.

Ferziger, J. H. and Peric, M., 1997, "Computational methods for fluid dynamics", Springer.

Fortuné, V., 2000, "Étude par Simulation Numérique Directe du rayonnement acoustique de couches de mélange isothermes et anisothermes", PhD thesis, Université de Poitier.

Germanos, R. A. C. and Medeiros, M. A. F., 2004, Simulação Numérica da Transição para Turbulência em uma Camada Limite Compressível sobre uma Placa Plana, 1º relatório técnico fapesp, Universidade de São Paulo - USP.

Germanos, R. A. C. and Medeiros, M. A. F., 2005, Simulação Numérica da Transição para Turbulência em uma Camada Limite Compressível sobre uma Placa Plana, 2º relatório técnico fapesp, Universidade de São Paulo - USP.

Germanos, R. A. C. and Medeiros, M. A. F., 2006, Simulação Numérica da Transição para Turbulência em uma Camada Limite Compressível sobre uma Placa Plana, 4º relatório técnico fapesp, Universidade de São Paulo - USP.

Germanos, R. A. C., Medeiros, M. A. F., and de Souza, L. F., 2004, Development of a computational code for studying compressible shear layer flow instabilities, "IV school of transition and turbulence".

Herbert, T., 1988, Secondary instability of boundary layers, "Ann. Rev. Fluid Mech.", Vol. 20, pp. 487–526.

Kloker, M., Rist, R., and Fasel, H., 1993, Outflow boundary conditions for spatial Navier-Stokes simulations of boundary layer transition, "AIAA J.", Vol. 31, pp. 620–628.

Kopal, Z., 1961, "Numerical Analysis", Wiley, New York.

Lele, S. K., 1992, Compact finite difference schemes with spectral-like resolution, "J. Comp. Phys.", Vol. **103**, pp. 16–42.

Lesieur, M., 1997, "Turbulence in fluids, (third edition)", Kluwer Academic Publisher.

Lessen, M., Fox, J. A., and Zien, H. N., 1966, Stability of the laminar Mixing of two Parallel Streams with respect to Supersonic Disturbances, "J. Fluid Mech.", Vol. 25, pp. 737–742.

Mahesh, K., 1998, A Family of High Order Finite Difference Schemes Spectral Resolution, "J. Comp. Phys.", Vol. **145**, pp. 332–358.

Medeiros, M. A. F., 2000, nonlinear hydrodynamic instability, "II school of transition and turbulence", pp.

312–357, Uberlândia – Brazil. in portuguese.

Medeiros, M. A. F., Silvestrini, J. H., and Mendonça, M. T., 2000, Using Linear and non Linear Stability Theory for Evaluating Code Accuracy, "II school of transition and turbulence".

Metcalfe, R., Orszag, S., Brachet, M., Menon, S., and Riley, J., 1987, Secondary instability of a temporally growing mixing layer, "J. Fluid Mech.", Vol. 184, pp. 207–243.

Michalke, A., 1964, On the instability of the hyperbolic-tangent velocity profile, "DVL-Institut für Turbulenzforschung, Berlin", pp. 543–556.

Papamoschou, D. and Roshko, A., 1988, The compressible turbulent mixing layer: an experimental study, "J. Fluid Mech.", Vol. **197**, pp. 453–477.

Rayleigh, L., 1880, On the stability, or instability, of certain fluid motions, "Proc. London Math. Soc.", Vol. 11, pp. 57–70.

Sandham, N. D. and Reynolds, W., 1989, Compressible Mixing Layer: Linear Theory and Direct Simulation, "AIAA Journal", Vol. 28, pp. 618–624.

Sandham, N. D. and Reynolds, W., 1991, Three-dimensional simulations of large eddies in the compressible mixing layer, "Journal of Fluids MEchanics", Vol. 224, pp. 133–158.

Souza, L. F., 2003, "Instabilidade centrífuga e transição para turbulência em escoamentos laminares sobre superfície côncava.", PhD thesis, Instituto Tecnológico de Aeronaútica, São José dos Campos - SP.

Souza, L. F., Mendonça, M. T., de Medeiros, M. A. F., and Kloker, M., 2002a, Analisys of Tollmien-Schlichting waves propagation on a flat plate with a Navier-Stokes solver, "9th brazilian congress on thermal engineering and sciences".

Souza, L. F., Mendonça, M. T., de Medeiros, M. A. F., and Kloker, M., 2002b, Three dimensional code validation for transition phenomena, "III Escola de Transição e Turbulência".

Souza, L. F., Mendonça, M. T., and Medeiros, M. A. F., 2002c, Assessment of Different Numerical Schemes and Grid Refinement for Hydrodynamic Stability Simulations, "ENCIT 2002", Campinas - SP.

Strang, G., 1988, "Linear Algebra and its applications.", HBJ.

Thompson, K. W., 1987, Time depedent boundary conditions for hyperbolic systems, "J. Comput. Phys.", Vol. 68, pp. 1–24.

White, F. M., 1974, "Viscous Fluid Flow, (First Edition)", McGraw-Hill.

Williamson, J. H., 1980, Low-storage Runge-Kutta Schemes, "J. Comp. Phys.", Vol. 35, pp. 48–56.